Journal of Applied Organometallic Chemistry
2023, Volume 3, Issue 4

Original Article

Improved Morphological, Structural, and Optical Features of Er_xCuNiO_3 {x= 0, 0.5, 0.7, 0.9}

Fawad Ali[a,b]| Imtiaz Ahmad[a,c]| Azmat Hussain[a,d]| Sadeeq Ahmad[a,d]| Muhammad Zaka Ansar[a]| Adezuka Yahaya[e]| Imosobomeh L. Ikhioya[a,e]*

[a]*National Centre for Physics, Quaid-i-Azam University Campus, Islamabad, 44000, Pakistan*
[b]*Department of Physics, Abbottabad University of Science and Technology, Abbottabad Islamabad, Pakistan*
[c]*Department of Physics, University of Engineering and Technology, Lahore, Pakistan*
[d]*Hazara University Mansehra, Pakistan*
[e]*Department of Physics, Federal College of Education, Okene, Kogi State, Nigeria*

Use your device to scan and read the article online

Citation F. Ali, I. Ahmad, A. Hussain, S. Ahmad, M.Z. Ansar, A. Yahaya, I.L. Ikhioya. **Improved Morphological, Structural, and Optical Features of Er_xCuNiO_3 {x= 0, 0.5, 0.7, 0.9}.** *J. Appl. Organomet. Chem.*, **2023**, *3*(4), 308-320.

https://doi.org/10.48309/JAOC.2023.421597.1127

Article info:
Received: 10 October 2023
Accepted: 12 November 2023
Available Online: 13 November 2023
ID: JAOC-2310-1127
Checked for Plagiarism: Yes
Language Editor checked: Yes

Keywords:
Erbium, Bandgap, Hydrothermal, Crystallite size, FTIR

ABSTRACT

To synthesize $ErCuNiO_3$, a 0.1 M solution of copper nitrate trihydrate ($Cu(NO_3)_2{\cdot}3H_2O$), nickel (II) nitrate hexahydrate $Ni(NO_3)_2{\cdot}6H_2O$, and sodium hydroxide (NaOH) were used. The (111) diffraction peak reveals the crystallization of the synthesized material. The presence of erbium in the $CuNiO_3$ lattice enhances the structure of the synthesized material, resulting in increased diffraction peaks. The synthesized $ErCuNiO_3$ reveals a cubic structure with diffraction peaks of (111), (101), (104) (112), (211), (222), and (311) corresponding to 2theta angle of 26.512°, 30.778°, 32.054°, 33.775°, 37.726°, 43.966°, and 44.989°, respectively. Introducing erbium into the lattice of the synthesized material results in an increase in the nanoparticle's size, increasing the surface area of the material. This increase in surface area enhances the material's photovoltaic activities. As the molar concentration of the material increases, the synthesized $ErCuNiO_3$ film exhibits a decrease in its indirect bandgap energy, which shifts from 1.50 eV to a range of 1.35-1.18 eV. The film exhibited a decrease in electrical conductivity, from 9.77 to 5.78 S/m, as its thickness increased from 107.00 to 115.35 nm, leading to an increase in resistivity from 10.23 to 17.35 Ω.cm.

Introduction

Nickel oxide has a cubic structure, and it falls under the category of p-type semiconductors and has an energy band gap of 3.6-4 eV [1]. Nickel oxide is used across a broad spectrum of applications, including solar cells, photocatalysis, sensors, and optical devices. CuO is a p-type semiconductor with an energy gap of 1.2 eV and a monoclinic structure [2]. Material scientists are paying a lot of attention to using combined composite semiconductor materials. Various applications for doped mineral oxide nanoparticles include magnetic semiconductors, photodetectors, and optoelectronics [3]. Excellent chemical stability and optical and electrical properties define this material. Two profitable materials in the field of semiconductors are nickel oxide and copper

Corresponding Authors: Imosobomeh L. Ikhioya (imosobomeh.ikhioya@unn.edu.ng)

oxide. Photovoltaic applications consider them for their exceptional performance and selectivity in reduction and oxidation reactions [4]. This material, which is a p-type semiconductor, comprises inexpensive and non-toxic elements. NiO is considered a leading p-type semiconductor of interest [5]. Nanostructured NiO material are widely used in electrochromic, energy storage, and photo electro-catalysis because of their stable electrochemical properties and easy processing [6]. Its appropriate band gap and energy level alignment make it a favored photocathode in Photo electrochemical water splitting applications. NiO is attracting interest in PEC cells because it can act as a proton reduction site and aid in charge carrier transport. NiO has limitations that should be addressed for efficient use as a photo-cathode in water splitting, despite its advantages [7]. The performance of the Photo electrochemical device is restricted by the small hole mobility and high charge carrier recombination rate at the NiO/electrolyte interface. Nanostructured materials are crucial for energy-storage devices because of their large surface area that aids in reactions [8]. The active material's crystal structure determines the speed of charging and discharging the electrode by affecting ion diffusion resistance. Shortening the diffusion path can reduce the resistance to diffusion in the solid phase. Thus, nano-sized materials effectively reduce diffusion resistance [9]. $ErCuNiO_3$ composites are important materials for energy storage, photovoltaic, and solar cell fabrication.

NiO-CuO films with a thickness of 200 nm were deposited on substrates at 400 °C using the chemical spray pyrolysis method [2]. The band gap decreases as the copper oxide mixing ratio increases. Optical properties maintain a constant absorption coefficient despite the variation in photon energy. The extinction coefficient was determined by wavelength for all films, and the refractive index increased with higher CuO content. The XRD results showed a polycrystalline structure with orientation in the (111) plane. Imran Khan *et al.* [10] present the synthesis of nickel oxide nanoparticles and Sr-doped nickel oxide nanoparticles using hydrothermal methods. Structural characterization techniques, such as XRD and SEM are used to analyze as-synthesized samples. Samples with low Sr dopant levels (1 to 2)% produce a cubic phase for the NiO-NPs. Sr doped NiO nanoparticles range in size from 50 to 100 nm, with decreased uniformity at higher dopant concentrations. By examining the electrical and dielectric properties of the synthesized material, they explore the influence of Sr dopant levels. Electrochemical studies have revealed that the chosen material have exceptional catalytic activity for glucose sensing, because of their unique structure and shape. Tuba Cayir Taşdemirc [3] used SILAR to make nanostructured undoped and Cu doped NiO thin films on glass. The optical analysis of undoped and Cu-doped NiO films showed a decrease in bandgap from 3.34 -2.01 eV with increasing Cu concentration. With the increase in Cu concentration, SEM analysis demonstrated changes in the shape of the nanostructures. The AFM analysis showed a decrease in surface roughness when copper was coated on the surface.

Different techniques can be used to deposit films, such as chemical vapor deposition, thermal evaporation, spin coating, and spray pyrolysis [4]. The report describes the synthesis of $ErCuNiO_3$ composite materials using a hydrothermal method. Synthesizing nanomaterials can be done through different methods. Pawar and Deshmukh emphasize the importance of the hydrothermal method in synthesizing thin films [11]. The hydrothermal method, a heterogeneous reaction, is performed using the autoclave. Place insoluble solutes in the autoclave and keep it in the oven below the supercritical point of water. Crystallization has led to the formation of thin films on the substrate, each with different shapes and sizes. Water serves as the primary solvent during the reaction. Variations in temperature and pressure unveil remarkable properties. Water's high density allows non-polar compounds to completely dissolve. This method can create different structures, such as three-dimensional nonospheres, two-dimensional nanosheets, and one-dimensional nanowires, by adjusting process parameters. Consistent composition and uniform shapes characterize these structures. Dissolving

insoluble materials at high temperature and pressure is the main purpose of this method. Advanced nanostructure preparation methods necessitate expensive instruments and surfactants. The byproduct produced by these methods has a negative impact on the environment. Pawar and Deshmukh claim that the hydrothermal method is environmentally friendly because it operates at low temperatures and does not need harmful catalysts [12]. Using this technique, material shape can be controlled and coatings can adhere well to various surfaces.

This paper assesses the impact of structure and optical properties on $ErCuNiO_3$ composites. The molar concentration of erbium was introduced to improve the material's photovoltaic properties.

Experimental

Materials

The materials used in this study are erbium (III) nitrate hexahydrate Sigma-Aldrich 99.9%, ($Er(NO_3)_3.6H_2O$), copper nitrate trihydrate ($Cu(NO_3)_2{\cdot}3H_2O$) Sigma-Aldrich 99.9%, Nickel (II) nitrate hexahydrate. $Ni(NO_3)_2{\cdot}6H_2O$ Sigma-Aldrich 99.9%, sodium hydroxide (NaOH), polyethylene glycol, α-terpineol, deionized water, heating mantle, and FTO-fluorine-doped tin oxide substrate, and also an oven that has a temperature range of 50 to 1000 °C.

$ErCuNiO_3$ synthesis

To synthesize $ErCuNiO_3$, a 0.1 M solution of copper nitrate trihydrate ($Cu(NO_3)_2{\cdot}3H_2O$), nickel (II) nitrate hexahydrate $Ni(NO_3)_2{\cdot}6H_2O$ and sodium hydroxide (NaOH) were used, and sodium hydroxide (NaOH) from Sigma-Aldrich, which was 99.0% pure, to 25 mL of deionized water and stirred it for 30 min at room temperature. Erbium (III) nitrate hexahydrate, ($Er(NO_3)_3{\cdot}6H_2O$) Sigma-Aldrich 99.9%, at a concentration of (0.5-0.9) M. To create a uniform solution, 1 g of polyethylene glycol and 1 g of *α*-terpineol were added to the mixed

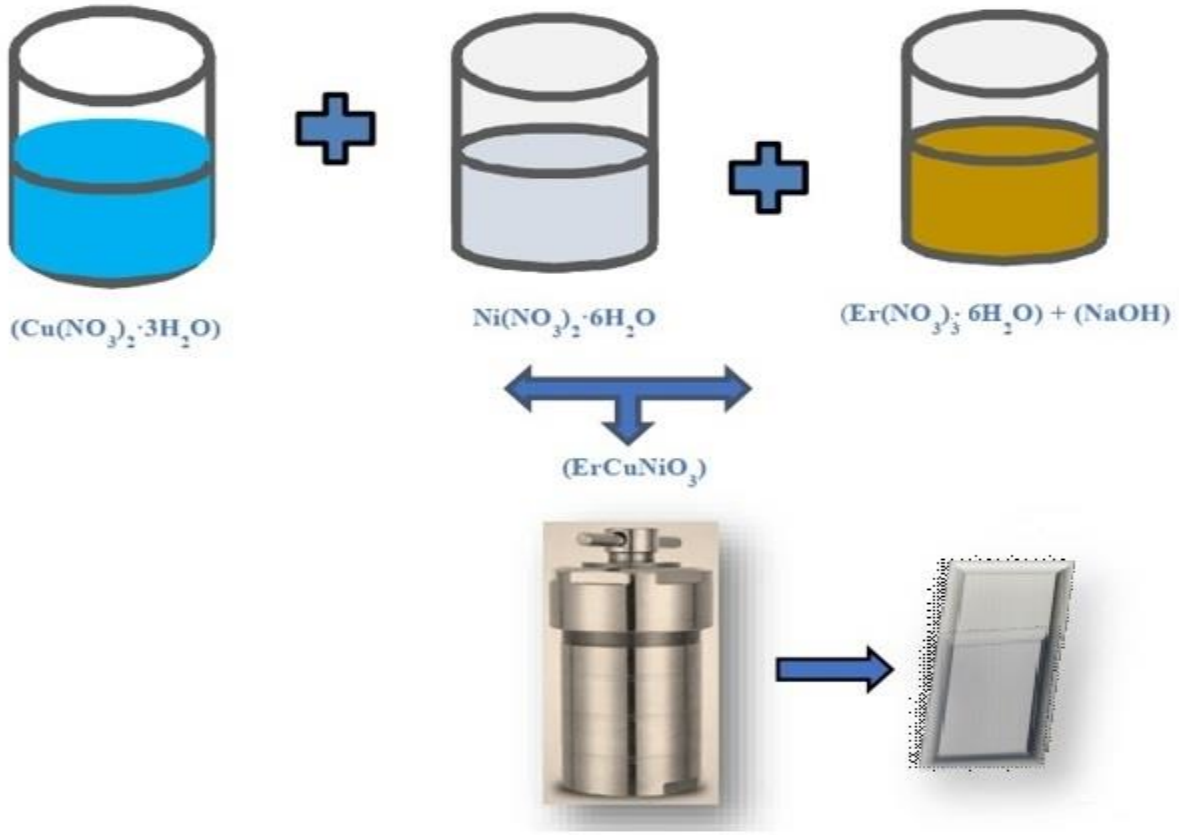

Figure 1. Schematic diagram of synthesis procedure

water and stirred it for 30 min at room temperature. Erbium (III) nitrate hexahydrate, ($Er(NO_3)_3 \cdot 6H_2O$) Sigma-Aldrich 99.9%, at a concentration of (0.5-0.9) M. To create a uniform solution, 1 g of polyethylene glycol and 1 g of α-terpineol were added to the mixed solutions and stirred for 30 minutes at room temperature. The FTO glass and solution were placed in a 100 ml Teflon-lined, stainless-steel autoclave for hydrothermal processing. The solution's temperature remained constant at 220 °C for 4 hours. The deposited $ErCuNiO_3$ on FTO substrate was vacuum-dried at 60 °C for 30 min after the autoclave cooled down naturally to room temperature (**Figure 1**). Various characterization techniques were employed to analyze the films, determining their optical, electrical, structural, morphological, and elemental compositions. The NPUFEI-NNS45 SEM was used to analyze structural and elemental compositions. The presence and types of functional groups in the $ErCuNiO_3$ films were examined using the JASCO-FTIR (FT/IR-6600). The films' absorbance wavelength was determined using a 756S UV-Visible spectrophotometer in the optical spectral range of 300 to 900 nm. We used the Jandel four-point probes method to analyze the electrical properties of the films.

Results and Discussion

Optical properties of $ErCuNiO_3$

Figure 2 (a) displays the absorbance spectra of the synthesized $ErCuNiO_3$. The absorption spectra showed a significant absorption rate between 300 and 900 nm. The presence of erbium in the $CuNiO_3$ lattice improves the absorption spectra of the synthesized $ErCuNiO_3$. The synthesis with 0.5 M has the highest absorption rate among all films. The films that have been synthesized with a 0.7 molar concentration of erbium show an improvement in performance compared to those with a lower concentration of erbium [2]. The absorbance rate of the synthesized material for photovoltaic use decreases with an increase in erbium concentration. A higher concentration of erbium results in a decreased absorption rate in the material. Introducing erbium may have caused a growth in crystallite size, as suggested by the decrease in crystallite peak observed in the XRD pattern. Decreasing the crystallite size can lead to a higher specific surface area and increased optical absorbance. The films are highly absorbent, making them ideal for solar cell technology and energy production. **Figure 2** (b) consistently exhibited a high rate of transmittance, with values even reaching 85%, particularly at a wavelength of 900 nm. In the infrared spectral region, $ErCuNiO_3$ demonstrates a high level of transmittance. The increase of the erbium concentration leads to a rise in the transmittance spectra. The films exhibited a rise in electrical resistivity, suggesting that this could be the cause. By enhancing the thickness of the film, there is a possibility that the specific surface area will increase, leading to potential improvement in optical transmittance. Because of their exceptionally high transmittance rate, these films are an ideal choice for various applications such as photovoltaics, energy production, and solar cell systems. **Figure 2** (c) revealed that the UV region had the highest reflectance. Upon evaluation, it was discovered that the films exhibited a low level of reflectance in both regions, which consequently makes them an ideal choice for both solar and photovoltaic cells. The negative reflectance observed in the material is caused by the interaction of light with the surface of the synthesized material, resulting in the effects interference and, ultimately, the cancellation of reflected light waves. They occur when the optical thickness of the material is overestimated. The estimate mentioned earlier may not fully account for the errors in the surface reflectance, as they can be larger than expected. This is mainly attributed to the influence of adjacency effects and the residuals that persist even after correction. The representation of the energy bandgap of $ErCuNiO_3$ can be observed in **Figure 2** (d) through the graph of $(\alpha hv)^2$ Vs hv. The utilization of the graph, which displayed the relationship between the absorption coefficient square and photon energy [13-20], allowed for the determination of indirect bandgap of the produced films. As the molar concentration of

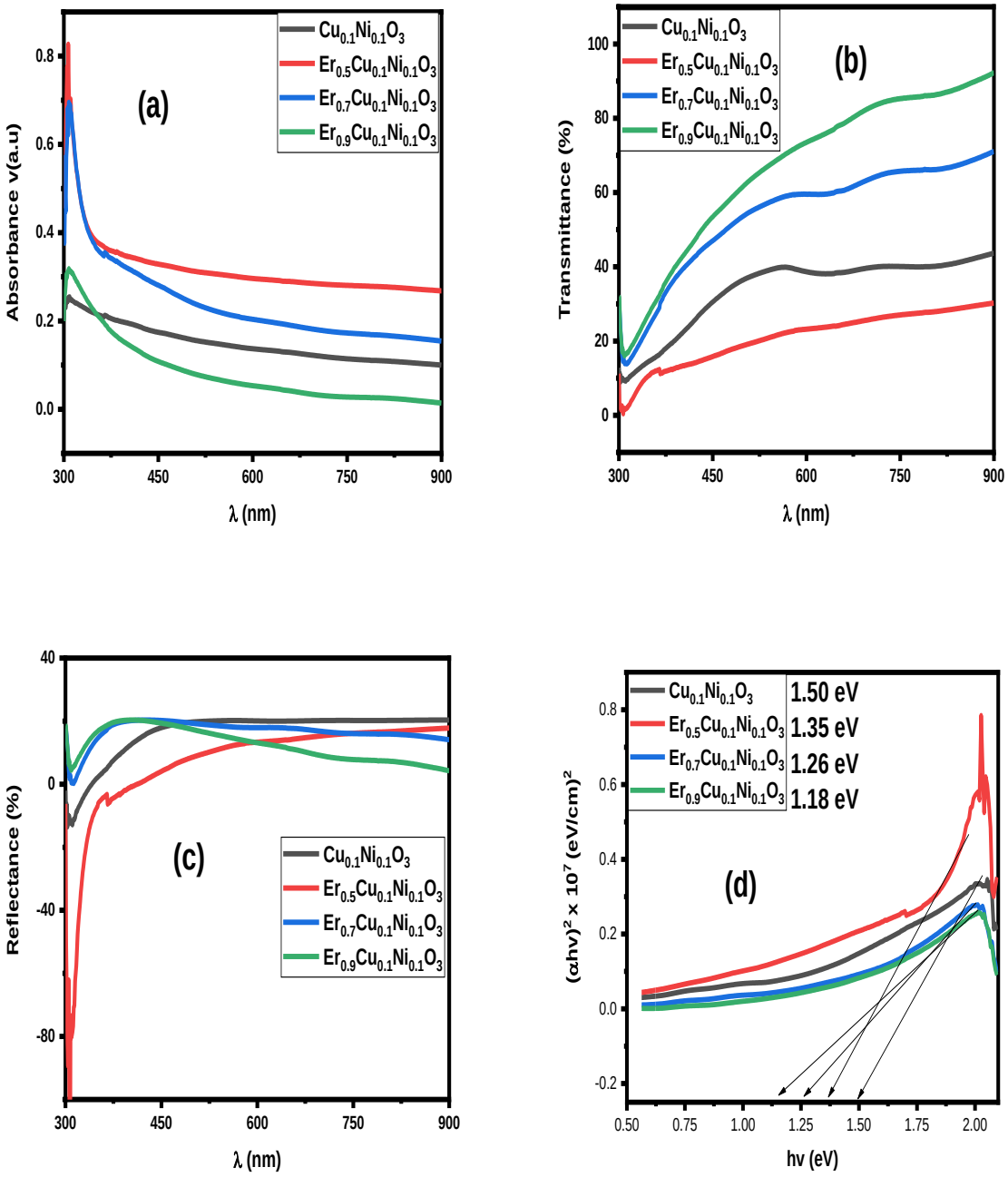

Figure 2. (a) absorbance, (b) transmittance, (c) reflectance, and (d) bandgap energy

the material increases, the synthesized $ErCuNiO_3$ film exhibits a decrease in its indirect bandgap energy, which shifts from 1.50 eV to a range of 1.35-1.18 eV.

Structural properties of ($ErCuNiO_3$)

The XRD pattern in **Figure 3** (a and b) displays the polycrystalline phase (cubic structure) of $CuNiO_3$ in the thin film. The (111), (112), and (211) diffraction peaks are observed at 2theta angles of 26.512°, 33.775°, and 37.726°, respectively. The (111) diffraction peak reveals the crystallization of the synthesized material. The presence of erbium in the $CuNiO_3$ lattice enhances the structure of the synthesized material, resulting in increased diffraction

peaks. The synthesized $ErCuNiO_3$ reveals a cubic structure with diffraction peaks of (111), (101), (104) (112), (211), (222), and (311) [13-20] corresponding to 2theta angle of 26.512°, 30.778°, 32.054°, 33.775°, 37.726°, 43.966, and 44.989°, respectively. In Table 1, the crystallite size of ErCuNiO3 decreases as the erbium concentration increases. The erbium concentration of 0.5, 0.7, and 0.9 M resulted in crystallite sizes of 2.3276, 2.2574, and 2.1913 nm, respectively. Different structural characteristics were determined by performing calculations using **Equations** (**1-4**) [7,9,21-29].

$$D = k\lambda/\beta \cos\theta \quad (1)$$

$$d = \lambda/2 \sin\theta \quad (2)$$

$$a = \sqrt{c^2/3} \quad (3)$$

$$c = \lambda/\sin\theta \quad (4)$$

Where, D is the crystallite size, λ is the wavelength, β is the full width at half maximum, d is the d-spacing, a is the lattice constant, and δ is the dislocation density. **Table 1** presents a correlation between the decrease in average crystallite size and the strain induced during hydrothermal process.

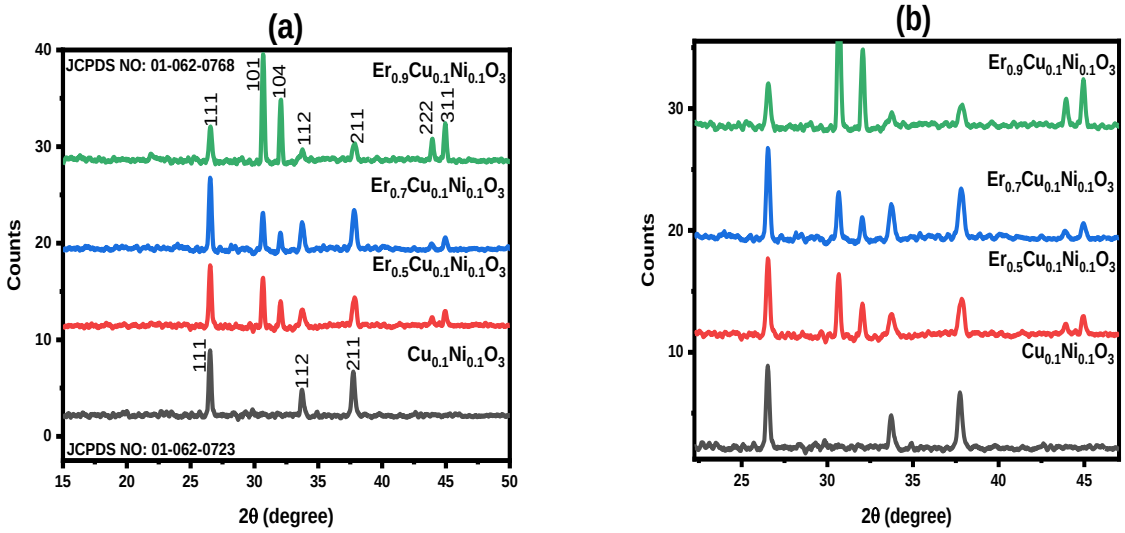

Figure 3. (a) XRD pattern and (b) magnified XRD pattern of the synthesized material

Table 1. Structural data of the synthesized material

+	2θ (degree)	(hkl)	d-spacing Å	a (Å)	FWHM (β)	Crystallite Size, D (nm)
$Cu_{0.1}Ni_{0.1}O_3$	26.512	111	3.3615	5.8223	0.4682	3.0448
	33.775	112	2.6534	5.3068	0.4693	3.0900
	37.726	211	2.3841	4.7682	0.4697	3.1219
$Er_{0.5}Cu_{0.1}Ni_{0.1}O_3$	26.512	111	3.3615	5.8223	0.6429	2.3276
	30.778	101	2.9046	5.0309	0.6442	2.3314
	32.054	104	2.7918	5.5836	0.6454	2.2720
	33.775	112	2.6534	5.3068	0.6456	2.3948
	37.726	211	2.3841	4.7682	0.6458	2.4259

Table 1. Continued

+	2θ (degree)	(hkl)	d-spacing Å	a (Å)	FWHM (β)	Crystallite Size, D (nm)
	43.966	222	2.0591	3.5665	0.6462	2.5094
	44.989	311	2.0146	4.0293	0.6464	2.5646
$Er_{0.7}Cu_{0.1}Ni_{0.1}O_3$	26.512	111	3.3615	5.8223	0.6629	2.2574
	30.778	101	2.9046	5.0309	0.6642	2.2612
	32.054	104	2.7918	5.5836	0.6654	2.2037
	33.775	112	2.6534	5.3068	0.6656	2.3228
	37.726	211	2.3841	4.7682	0.6658	2.3531
	43.966	222	2.0591	3.5665	0.6462	2.5094
	44.989	311	2.0146	4.0293	0.6664	2.4876
$Er_{0.9}Cu_{0.1}Ni_{0.1}O_3$	26.512	111	3.3615	5.8223	0.6829	2.1913
	30.778	101	2.9046	5.0309	0.6842	2.1951
	32.054	104	2.7918	5.5836	0.6854	2.1394
	33.775	112	2.6534	5.3068	0.6856	2.2551
	37.726	211	2.3841	4.7682	0.6658	2.3531
	43.966	222	2.0591	3.5665	0.6662	2.4340
	44.989	311	2.0146	4.0293	0.6864	2.4151

Surface morphology of the synthesized material

The surface morphology of $ErCuNiO_3$ is depicted in **Figure 4**. Small nanoparticles and significant nano wax particles are both observable in the $CuNiO_3$ material. Including erbium in the material causes the nanoparticles to grow and expand the surface area. This increase in surface area enhances the material's photovoltaic activities. More erbium concentration leads to higher surface energy because of nanoparticle clusters. The surface area of the synthesized films for energy storage activities is increased by a high molar concentration of erbium. Because of the strain, there was a change in the lattice's orientation, which consequently led to a reduction in the size of the material's crystallite [13-20]. **Figure 5** demonstrates the elemental composition of $ErCuNiO_3$. All essential elements for the $ErCuNiO_3$ formation are clearly depicted in the spectrum. The composition of FTO substrate used in the synthesis procedure was also considered. The details of the percentage weight of the element present in the EDX analysis can be observed in **Table 2**.

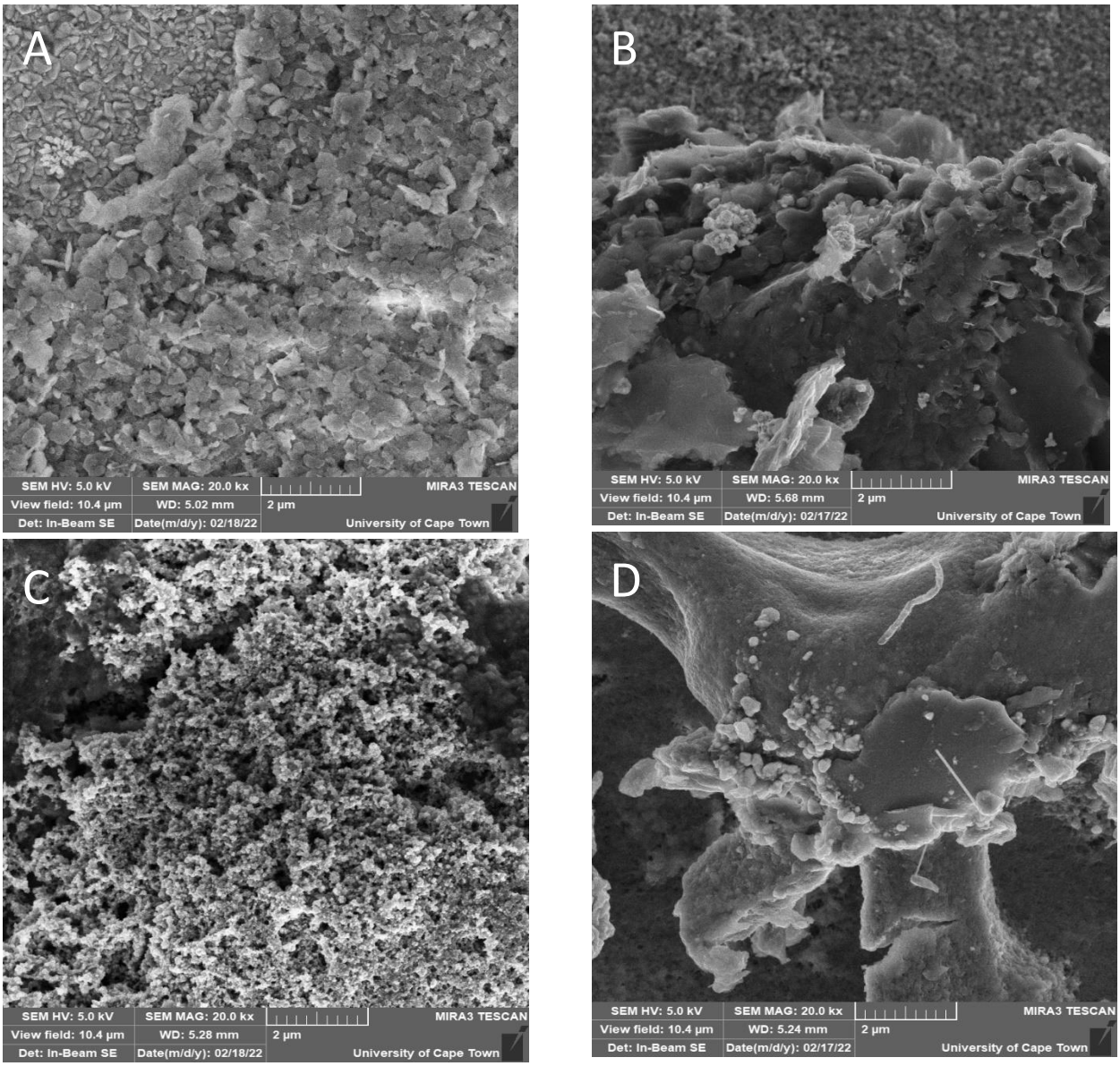

Figure 4. (A) $Cu_{0.1}Ni_{0.1}O_3$, (B) $Er_{0.5}Cu_{0.1}Ni_{0.1}O_3$, (C) $Er_{0.7}Cu_{0.1}Ni_{0.1}O_3$, and (D) $Er_{0.9}Cu_{0.1}Ni_{0.1}O_3$

Table 2. EDX spectra atomic weight percentages of the constituent elements

$Cu_{0.1}Ni_{0.1}O_3$		$Er_{0.5}Cu_{0.1}Ni_{0.1}O_3$	
Component	**Atomic Weight (%)**	**Component**	**Atomic Weight (%)**
Cu	57.00	Cu	57.00
Ni	23.01	Ni	21.00
O	13.50	O	10.00
Ca	2.99	Ca	1.00
Si	3.50	Si	2.00
-	-	Er	9.20

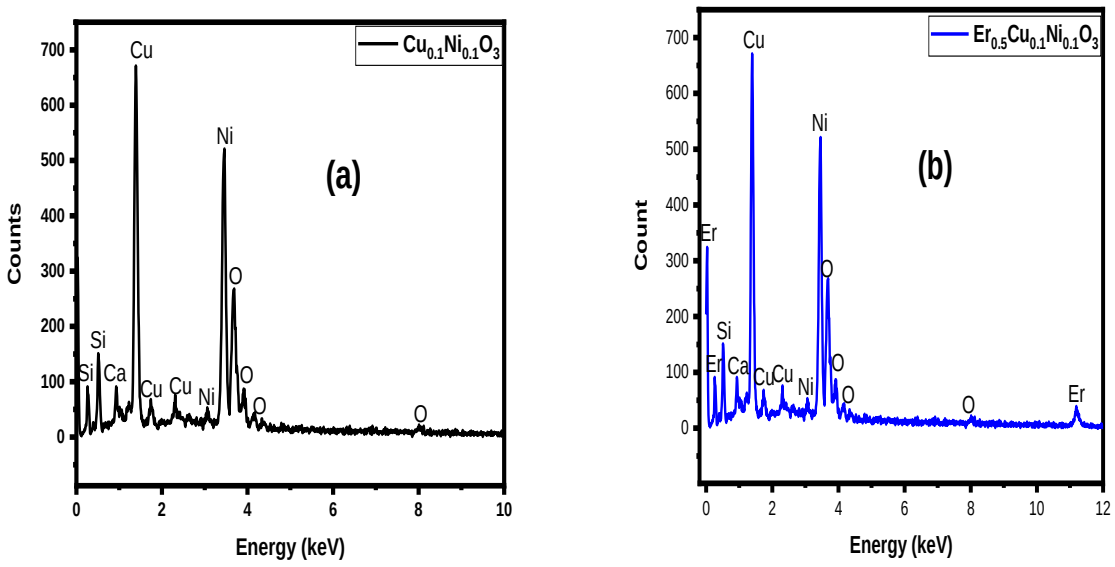

Figure 5. EDX spectrum of (a) $Cu_{0.1}Ni_{0.1}O_3$ and (b) $Er_{0.5}Cu_{0.1}Ni_{0.1}O_3$

Electrical properties of the synthesized $ErCu_{0.1}Ni_{0.1}O_3$

Figure 6 reveals the relationship between film thickness and electrical resistivity or conductivity. When the film thickness is increased, it leads to an increase in electrical resistivity and a simultaneous decrease in the conductivity of the films. The alignment occurs because erbium is introduced, resulting in an increase in carrier concentration and ultimately enhancing electrical conductivity. The beneficial aspect of the material lies in its ability to handle a greater amount of electric current, which is helpful for various optoelectronic applications [13-20]. The analysis of resistivity and conductivity for $ErCu_{0.1}Ni_{0.1}O_3$ is presented in **Table 3**, providing valuable insights into the electrical properties of this material. The film exhibited a decrease in electrical conductivity, from 9.77 to 5.78 S/m, as its thickness increased from 107.00 to 115.35 nm, leading to an increase in resistivity from 10.23 to 17.35 Ω.cm. The erbium lattice has a direct impact on the electron-hole pairs found in $ErCu_{0.1}Ni_{0.1}O$, resulting in an alteration in the spacing between them because of the crystallite size. The variation in crystallite sizes between the Erbium molar concentration and $Cu_{0.1}Ni_{0.1}O$ led to a reduction in the electrical conductivity of the films. The increase in resistivity and film thickness of $ErCu_{0.1}Ni_{0.1}O$ is correlated with the concentration of erbium. The potential value of this film lies in its ability to enhance solar cell efficiency. $ErCu_{0.1}Ni_{0.1}O_3$, exhibits a resistivity that is highly suitable for use as buffer layers in photovoltaic systems.

Table 3. Electrical properties of $ErCuNiO_3$

Films	Thickness, t (nm)	Resistivity, ρ (Ω.cm) × 10^6	Conductivity, σ (S/m) × 10^4
$Cu_{0.1}Ni_{0.1}O_3$	107.00	10.23	9.77
$Er_{0.5}Cu_{0.1}Ni_{0.1}O_3$	109.23	13.00	7.69
$Er_{0.7}Cu_{0.1}Ni_{0.1}O_3$	113.32	16.24	6.15
$Er_{0.9}Cu_{0.1}Ni_{0.1}O_3$	115.35	17.30	5.78

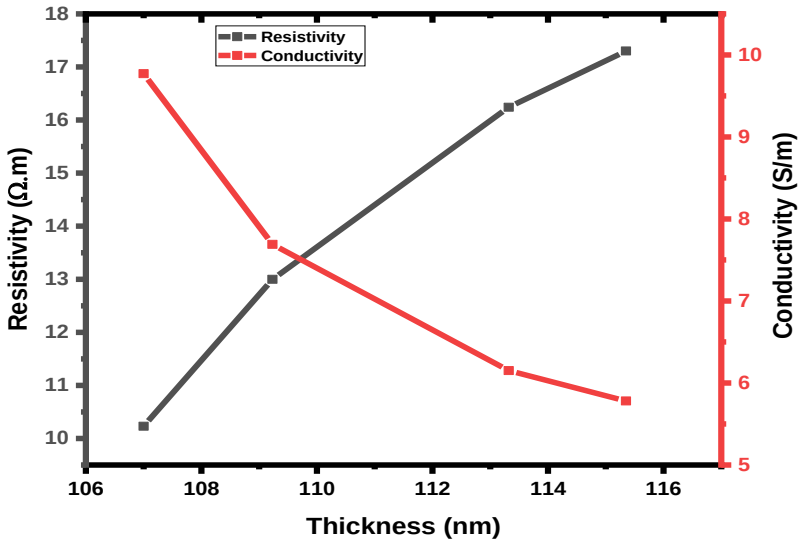

Figure 6. Plot of resistivity and conductivity of $ErCu_{0.1}Ni_{0.1}O_3$

FTIR analysis of $ErCu_{0.1}Ni_{0.1}O_3$

In this study, the FTIR spectra of $ErCu_{0.1}Ni_{0.1}O_3$ are being investigated to determine the unique properties of the synthesize films in **Figure 7**. By increasing the erbium molar concentration in the films, Er^{2+}, Cu^{2+} ions can be detected, causing a symmetrical peak to appear at 779 cm^{-1}. The binding of O-H to nickel causes this peak. A common trend can be observed in all films, whereby the 779 cm^{-1} band in the asymmetrically stretched carbonates ion at 1354 cm^{-1} decreases as the concentration increases. Atmospheric CO_2 handles the band observed at approximately 1582 cm^{-1} in the spectra. The presence of a peak at approximately 1005 cm^{-1} shows the Ni-O stretching vibrations in the compound $ErCu_{0.1}Ni_{0.1}O_3$. The material went through this change because of an increase in the volume of its unit cell. The observed strong absorption band, which is at approximately 1005 cm^{-1}, is the caused by the bending vibration of the oxygen octahedral deformation mode.

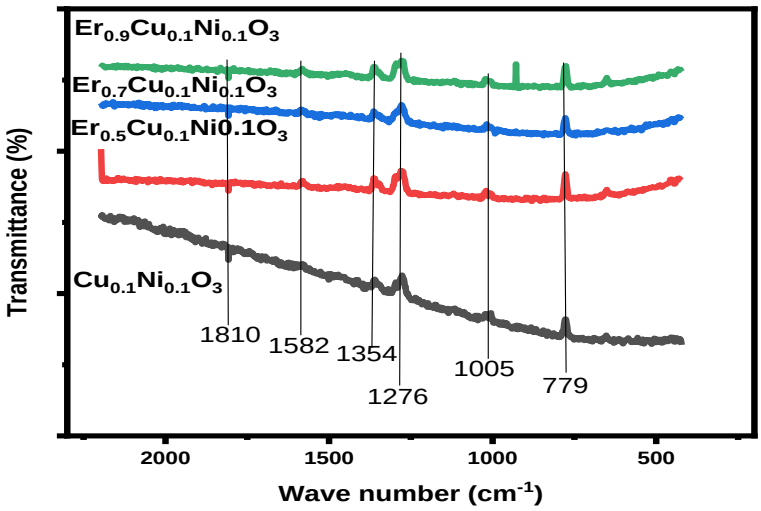

Figure 7. Plot of FTIR of $ErCu_{0.1}Ni_{0.1}O_3$

Conclusion

Using a hydrothermal approach, we have successfully synthesized $ErCuNiO_3$. The absorption spectra showed a significant absorption rate between 300 and 900 nm. Erbium in the $CuNiO_3$ lattice enhances the absorption spectra of $ErCuNiO_3$. The synthesis with 0.5 M exhibits the highest absorption rate compared to other films. The (111) diffraction peak reveals the crystallization of the synthesized material. The presence of erbium in the $CuNiO_3$ lattice enhances the structure of the synthesized material, resulting in increased diffraction peaks. The synthesized $ErCuNiO_3$ reveals a cubic structure with diffraction peaks of (111), (101), (104) (112), (211), (222), and (311) corresponding to 2theta angle of 26.512°, 30.778°, 32.054°, 33.775°, 37.726°, 43.966°, and 44.989°, respectively. Introducing erbium into the lattice of the synthesized material results in an increase in the nanoparticle's size, increasing the surface area of the material. This increase in surface area enhances the material's photovoltaic activities. As the molar concentration of the material increases, the synthesized $ErCuNiO_3$ film exhibits a decrease in its indirect bandgap energy, which shifts from 1.50 eV to a range of 1.35-1.18 eV. The film exhibited a decrease in electrical conductivity, from 9.77 to 5.78 S/m, as its thickness increased from 107.00 to 115.35 nm, leading to an increase in resistivity from 10.23 to 17.35 Ω.cm.

Disclosure Statement

The authors state they have no personal or financial conflicts that could have influenced the research in this article.

Acknowledgments

We extend our gratitude to all the authors for their significant contributions to the success of the paper.

Orcid

Imosobomeh L. Ikhioya
https://orcid.org/0000-0002-5959-4427

References

[1]. A. Emamdoust, S. Farjami Shayesteh, Surface and electrochemical properties of flower-like Cu-NiO compounds, *Journal of Alloys and Compounds*, **2018**, *738*, 432–439. [Crossref], [Google Scholar], [Publisher]

[2]. Z.T. Khodair, M.A. Al-Jubbori, A.M. Shano, F.I. Sharrad, Study of optical and structural properties of $(NiO)_{1-x}(CuO)_x$ nanostructures thin films, *Chemical Data Collections*, **2020**, *28*, 100414. [Crossref], [Google Scholar], [Publisher]

[3]. T. ÇAYIR TAŞDEMİRCİ, Synthesis of copper-doped nickel oxide thin films: Structural and optical studies, *Chemical Physics Letters*, **2020**, *738*, 136884. [Crossref], [Google Scholar], [Publisher]

[4]. N. Effendy, Z.A. Wahab, S.H.A. Aziz, K.A. Matori, M.H.M. Zaid, S.S.A. Rashid, Characterization and optical properties of erbium oxide doped ZNO–SLS glass for potential optical and optoelectronic materials, *Materials Express*, **2017**, *7*, 59–65. [Crossref], [Google Scholar], [Publisher]

[5]. H. Liu, G. Yan, F. Liu, Y. Zhong, B. Feng, Structural, electrochemical and optical properties of NiO_xH_y thin films prepared by electrochemical deposition, *Journal of Alloys and Compounds*, **2009**, *481*, 385–389. [Crossref], [Google Scholar], [Publisher]

[6]. P. Sahoo, A. Sharma, S. Padhan, R. Thangavel, Cu doped NiO thin film photocathodes for enhanced PEC performance, *Superlattices and Microstructures*, **2021**, *159*, 107050. [Crossref], [Google Scholar], [Publisher]

[7]. D.C. Okeudo *et al.,* Influence of polyethylene glycol (PEG) surfactant on the properties of molybdenum-doped zinc oxide films, *Journal of Nano and Materials Science Research*, **2023**, *2*, 83–89. [Google Scholar], [Publisher]

[8]. M. Salavati-Niasari, N. Mir, F. Davar, A novel precursor in preparation and characterization of nickel oxide nanoparticles via thermal decomposition approach, *Journal of Alloys and*

Compounds, **2010**, *493*, 1–2, 163–168. [Crossref], [Google Scholar], [Publisher]

[9]. H. Shah, S. Afzal, M. Usman, K. Shahzad, I. L. Ikhioya, Impact of annealing temperature on lanthanum erbium telluride ($La_{0.1}Er_{0.2}Te_{0.2}$) nanoparticles synthesized via hydrothermal approach, *Advanced Journal of Chemistry, Section A*, **2023**, *6*, 342–351. [Crossref], [Google Scholar], [Publisher]

[10]. W. Abbas *et al.,* Study of the electrical properties and electrochemical sensing efficiency of hydrothermally synthesized Sr doped Nickel oxide nanomaterials, *Physica Scripta*, **2022**, *97*, 075004. [Crossref], [Google Scholar], [Publisher]

[11]. P.B. Patil *et al.,* Single step hydrothermal synthesis of hierarchical TiO_2 microflowers with radially assembled nanorods for enhanced photovoltaic performance, *RSC Advances*, **2014**, *4*, 7278–47286. [Crossref], [Google Scholar], [Publisher]

[12]. M.D. Jeroh, A.J. Ekpunobi, D.N. Okoli, Optical analytical studies of Electrostatic sprayed Eu-doped Cadmium selenide nanofilms at different temperatures, *Journal of nano and electronic physics*, **2018**, *10*. [Crossref], [Google Scholar], [Publisher]

[13]. N.A. Okereke, A.J. Ekpunobi, XRD and UV-VIS-IR studies of chemically-synthesized copper selenide thin films, *Research Journal of Chemical Sciences*, **2011**, *1*, 64-70. [Crossref], [Google Scholar]

[14]. I.L. Ikhioya, O.B. Uyoyou, A.L. Oghenerivwe, The effect of molybdenum-doped tin selenide semiconductor material (SnSe) synthesized via electrochemical deposition technique for photovoltaic application, *Journal of Materials Science: Materials in Electronics*, **2022**, *33*, 10379–10387. [Crossref], [Google Scholar], [Publisher]

[15]. a) N.I. Akpu, *et al.,* Investigation on the influence of varying substrate temperature on the physical features of yttrium doped cadmium selenide thin films materials, *SSRG International Journal of Applied Physics*, **2021**, *8*, 37-46. [Crossref], [Google Scholar], [Publisher] b) A. Johnson, Investigating the effects of environmental applications on decomposition of zein nanoparticles in adsorbents in industry, *Journal of Engineering in Industrial Research*, **2023**, *4*, 93-109. [Crossref], [Publisher]

[16]. I.L. Ikhioya, E. Danladi, O.D. Nnanyere, A.O. Salawu, Influence of precursor temperature on bi doped ZnSe material via electrochemical deposition technique for photovoltaic application, *Journal of the Nigerian Society of Physical Sciences*, **2022**, *4*, 123–129. [Crossref], [Google Scholar], [Publisher]

[17]. a) A.N. Ifeyinwa, A.O. Maxwell, O.C. Julia, I.L. Ikhioya, Growth and optimization of physical properties of cadmium selenide semiconductor material via yttrium doping for photovoltaic / solar energy purposes, *Journal of Materials and Environmental Science*, **2022**, *13*, 681–691. [Crossref], [Google Scholar], [Publisher] b) A.I. Agbrara, E.O. Ojegu, M.O. Osiele, I. Ikhioya, Electrochemically synthesize SrSe/ZrSe heterostructure material for photovoltaic application, *Advanced Journal of Chemistry, Section A*, **2023**, *6*, 401-411. [Crossref], [Google Scholar], [Publisher]

[18]. A.A Yadav, Nanocrystalline copper selenide thin films by chemical spray pyrolysis, *Journal of Materials Science: Materials in Electronics*, **2014**, *25*, 1251–1257. [Crossref], [Google Scholar], [Publisher]

[19]. J. Allen *et al.,* Binder-free fabricated $CuFeS_2$ electrodes for supercapacitor applications, *Materials Research Express*, **2022**, *9*, 025501. [Crossref], [Google Scholar], [Publisher]

[20]. N.I. Akpu, A.D. Asiegbu, L.A. Nnanna, I.L. Ikhioya, T.I. Mgbeojedo, Influence of substrate temperature on the photovoltaic/optoelectronic properties of spray-synthesized yttrium copper selenide (YCS) thin films, *Arabian Journal for Science and Engineering*, **2022**, *47*, 7639–7646. [Crossref], [Google Scholar], [Publisher]

[21]. B.C.N. Obitte, I.L. Ikhioya, G.M. Whyte, U.K. Chime, B.A. Ezekoye, A.B.C. Ekwealor, M. Maaza, Fabian I. Ezema, The effects of doping and temperature on properties of electrochemically deposited Er^{3+} doped ZnSe thin films, *Optical Materials*, **2022**, *124*, 111970. [Crossref], [Google Scholar], [Publisher]

[22]. J.M. Rzaij, A.M. Abass, Review on: TiO_2 thin film as a metal oxide gas sensor, *Journal of Chemical Reviews*, **2020**, *2*, 114-121. [Crossref], [Google Scholar], [Publisher]

[23]. G. Govindasamy, Murugasen, S. Sagadevan, Optical and electrical properties of chemical bath deposited cobalt sulphide thin films, *Materials Research*, **2016**, 0441. [Crossref], [Google Scholar], [Publisher]

[24]. F. Liu, B. Wang, Y. Lai, J. Li, Z. Zhang, Y. Liu, Electrodeposition of cobalt selenide thin films, *Journal of The Electrochemical Society*, **2010**, *157*, D523-D527. [Crossref], [Google Scholar], [Publisher]

[25]. E.N. Josephine, O.S. Ikponmwosa, I.L. Ikhioya, Synthesis of SnS/SnO nanostructure material for photovoltaic application, *East European Journal of Physics*, **2023**, *2023*, 154–161. [Crossref], [Google Scholar], [Publisher]

[26]. J. Koo Kima, J. Hwa Kimb, Y. Chan Kanga, Electrochemical properties of multicomponent oxide and selenide microspheres containing Co and Mo components with several tens of vacant nano rooms synthesized by spray pyrolysis, *Chemical Engineering Journal*, **2018**, *333*, 665-677. [Crossref], [Google Scholar], [Publisher]

[27]. P.E. Agbo, P.A. Nwofe, R.A. Chikwenze, D.A Famuyibo, Effect of pH on properties of CoSe thin films deposited by chemical bath technique, *African Journal of Basic & Applied Sciences*, **2016**, *8*, 152-156. [Crossref], [Google Scholar], [Publisher]

[28]. K.I. Udofia, D.N. Okoli, Investigation of the optical, structural and surface morphology properties of Copper selenide thin film, *International Journal of Scientific Research and Education*, **2017**, *5*, 6357–6363. [Crossref], [Google Scholar], [Publisher]

[29]. M.R. Zamani Meymian, M. Moradi Haji M. Jafan, Rabbani, M. Behboudnia, Improving the morphology and electro-optic properties of ITO thin film, by changing argon rate and atmosphere pressure, *Asian Journal of Green Chemistry*, **2022**, *6*, 175-184. [Crossref], [Publisher]